atmosphere

MDPI

Article

The Comprehensive Study of Low Thermospheric Sodium Layers during the 24th Solar Cycle

Yuchang Xun [1,2,3], Guotao Yang [2,*], Jihong Wang [2], Lifang Du [2], Zelong Wang [2,4], Jing Jiao [2], Xuewu Cheng [5], Faquan Li [5] and Xu Zou [6]

1 College of Physics and Optoelectronics, Taiyuan University of Technology, Taiyuan 030024, China; xunyuchang@tyut.edu.cn
2 State Key Laboratory of Space Weather, National Space Science Center, Chinese Academy of Sciences, Beijing 100190, China; jhwang@nssc.ac.cn (J.W.); lfdu@nssc.ac.cn (L.D.); zlwang@jnu.edu.cn (Z.W.); jjiao@swl.ac.cn (J.J.)
3 Key Laboratory of Advanced Transducers and Intelligent Control Systems, Ministry of Education and Shanxi Province, Taiyuan University of Technology, Taiyuan 030024, China
4 Institute for Environmental and Climate Research, Jinan University, Guangzhou 511443, China
5 Wuhan Institute of Physics and Mathematics, Chinese Academy of Sciences, Wuhan 430071, China; lidar@wipm.ac.cn (X.C.); lifaquan@wipm.ac.cn (F.L.)
6 Department of Physics and Electronic Engineering, Hainan Normal University, Haikou 571158, China; christian5022@163.com
* Correspondence: gtyang@nssc.ac.cn

Received: 23 January 2020; Accepted: 9 March 2020; Published: 14 March 2020

check for updates

Abstract: The low thermospheric sodium layer (LTSL) is the separate sodium atom layer above 105 km. Based on 11,607 h of lidar observations from Yanqing (40.5° N, 116.0° E) from 2010 to 2016, we found 38 LTSLs wherein the peak densities were more than five percent above those of the main sodium layers. This work presents the peak altitudes, peak local times and peak densities of the LTSLs as well as the long-term characteristics of the seasonal and inter-annual variations of LTSLs. We analyzed the correlation between the LTSL and sporadic E layer (Es). The seasonal variation trends of the occurrences of LTSL and Es are similar, and the results showed that 95% of the LTSLs were accompanied by Es. We also found that 69% of the LTSL cases exhibited apparent downward phase progressions, while the descending rates of the LTSLs are consistent with the phase speeds of the tide.

Keywords: low thermospheric sodium layer; sporadic E layer; tide

1. Introduction

The first report about the Na D line being present in the night sky spectrum was by Slipher et al. [1]. From then on, large studies of the sodium layer have been conducted using airglow imager and lidar data. Sodium atoms are mainly distributed from 80 km to 105 km and are caused by various neutral and ionic chemical reactions between sodium species and other atmospheric constituents. Sodium atoms will be oxidized at lower altitudes and ionized at higher altitudes, with the free sodium atoms being located at approximately 90 km [2].

Later, researchers found that the density of the sodium atoms can increase and decrease suddenly over a narrow height range. This phenomenon was called the sporadic sodium layer (SSL). As early as 1978, the first SSL was observed by Clemesha at Sao Jose dos Campos (23° S, 46° W) [3]. Afterwards, many SSLs were found in low, middle and high latitude regions [4–10]. Most SSLs appeared to occur around midnight local time and were located above 90 km. The full width at half maximum (FWHM) of the SSL was less than 5 km, and the peak value of the SSL was generally several times larger than that of the background sodium layer [11]. Furthermore, the occurrence rates, central heights and densities of the SSLs had obvious seasonal variations [12]. The most accepted explanation for the SSL formation is the neutralization of sodium ions in the sporadic E layer (Es), while formations related to meteor injections, auroral particle precipitation, and temperature increases were also proposed [10,13–16].

Over the past twenty years, a much unexpected sodium density increase feature was found in the low thermosphere via lidar data. Collins et al first reported "a large sporadic sodium layer near 109 km" with a peak density close to the peak density of the main sodium layer that lasted 15 min and was found at Poker Flat, Alaska (67° N, 147° W), during an active aurora [17]. Gong et al. reported a two-hour "double sodium layer" with a peak density of approximately 25% that of the main sodium layer located at 112 km in Wuhan (31° N, 147° E) [18]. In recent years, researchers have observed several similar LTSLs at high, middle, and low latitudes. These LTSLs have instigated considerable and prolonged concern. Wang et al. reported 17 "double sodium layers" (105 km–130 km) over Beijing, China, during 2009–2011 [19]. Xue et al. reported two "thermospheric enhanced sodium layers" separate from the main layer at approximately 120 km with densities an order of magnitude less than the peak density on 10 March and 10 April 2012 at Lijiang (26.7° N, 100.0° E), China [20]. Dou et al. compared the peak densities, peak altitudes, FWHMs, and peak times of the "thermospheric enhanced sodium layers" observed at Beijing (40.2° N, 116.2° E), Hefei (31.8° N, 117.3° E), Wuhan (30.5° N, 144.4° E), and Haikou (19.5° N, 109.1° E) [21]. Ma et al. surveyed 11 "high-altitude (above 105 km) sporadic sodium events" at Qingdao (36° N, 120° E), China, based on 430 h of data from December 2007 to June 2012 and these separated sodium layers are called low thermospheric sodium layers (LTSL) [22].

Moreover, the latest research reported the presence of sodium layers at higher altitudes. Tsuda et al. reported "a thermospheric sodium layer event at up to 140 km" observed on the night of 23–24 September 2000 at Syowa (69.0° S, 39.6° E), Antarctica [23]. Gao et al. reported "thermospheric sodium layers at up to 170 km" in March, April, and December 2012 over Lijiang (26.7° N, 100.0° E), China [24]. Liu et al. described the case of "thermospheric sodium atoms" appearing up to 160 km on 17 April 2015 at Cerro Pachón, Chile (30.25° S, 70.74° W) [25]. Xun et al. reported "thermospheric Na layers reached 200 km" on 05 February 2018 at Yanqing [26]. Furthermore, iron and potassium atom layers were also reported above 140 km [27–29].

LTSLs have greatly invoked interest because sodium ions are very difficult to neutralize above 105 km due to the ratio of CO_2:O being too small [16]. Thus, researchers have tried to determine how to accelerate the neutralization of sodium ions. Xue et al. found an Es layer before the "thermospheric enhanced sodium layers", and these sodium layers are formed through the tidal wind shear mechanism [20]. Yuan et al. suggested that at a tidal wind shear node, increased atmospheric pressure and density components contribute to the formation of Es and "high-altitude sporadic sodium layers" [30]. Chu et al. reported that electric fields during auroras can accelerate the formation of Es layers, and the related metal atoms can be neutralized and prevented from converging with metal ions [27]. Tsuda et al. demonstrated that the observed thermospheric sodium atoms follow this pattern [23]. In 2017, Chu developed a thermosphere-iomosphere Fe/Fe+ model to depict the lifecycle of metals via deposition, transport, chemistry and wave dynamics in the polar regions [31]. And Cai et al. Developed the numerical simulation covered the horizontal transport, fountain effect, and recombination effect to investigate the generation of the thermospheric sodium atoms [32,33].

Several case studies mentioned above have noted that the LTSLs are accompanied by the appearances of Es and the specific conditions at a tidal wind shear node will accelerate the formation of an LTSL. Due to the extremely low occurrence frequencies of LTSLs, there has been no systematic statistical study of the correlations among the LTSLs, Es and tidal wave. Therefore, we still lack an understanding of the LTSLs. Does this phenomenon have regular seasonal changes or inter-annual variability? Is there a direct relation between the LTSL and the Es or the LTSL and tidal wave?

In this paper, we report the extensive analyses on over 11,600 h of broadband Na lidar observations made near Beijing to look for thermospheric Na layers above 105 km. In Section 2, the observational data is described. The statistical analyses of the peak altitudes, peak local times, FWHMs, and peak densities of the LTSLs are presented in Section 3. Meanwhile, we discuss the seasonal and inter-annual variations of the LTSLs, and the relationships among the LTSLs, Es and tidal wave. Finally, the conclusions of this study are provided in Section 4.

2. Data Sources

The sodium density data comes from the data center for Meridian Space Weather Monitoring Project [34]. The lidar system is located at Yanqing (40.5° N, 116.0° E) Station. The sodium lidar pulses at 589 nm were produced by a tunable dye laser pumped by the second harmonic of an Nd: YAG (neodymium-doped yttrium aluminum garnet) laser at 532 nm, with a telescope diameter of 1000 mm. The lidar system parameters of Yanqing lidar have been given by Jiao et al., and Wang et al, [35,36]. The temporal and spatial resolutions of the lidar are 2.8 min and 96 m, respectively.

The ionospheric data and atmospheric wind data were taken from the Institute of Geology and Geophysics, Chinese Academy of Science, specifically from ionosonde and meteor radar located at Shisanling (40.3° N, 116.2° E) Station. The direct distance between Yanqing Station and Shisanling Station is approximately 30 km. The temporal resolution of the ionosonde is 15 min, and the temporal and spatial resolutions of the meteor radar are 1 h and 2 km, respectively.

The daily number of sunspots comes from the World Data Center for the Production, Preservation and Dissemination of the International Sunspot Number.

3. Results and Discussion

3.1. Statistical Results

3.1.1. The Parameters of the LTSLs

The LTSLs were selected according to the following criteria: The peak altitude of the LTSL is higher than 105 km [18,19]; the LTSL is separated from the main sodium layer [21]. To identify more typical LTSLs, we added two additional criteria: The LTSL lasts at least one hour from its formation to its disappearance for the observations or until it merges into the main sodium layer below 105 km; and when the LTSL appeared at its highest altitude, the peak density of the LTSL is greater than one-twentieth of the peak density of the main sodium layer. Figure 1 shows an LTSL case from 6 July 2010.

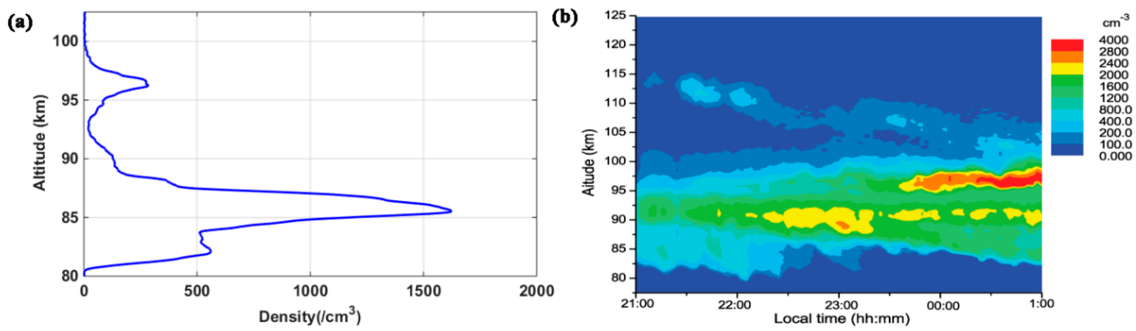

Figure 1. (**a**) The profile of the sodium density at 21:34 LT (Local Time) on 6 July 2010 and (**b**) the time-altitude variations of the sodium density from 21:00 LT on 6 July 2010 to 01:00 LT on 7 July 2010.

Figure 1a exemplifies an LTSL case. In this case, the main sodium layer extended 80 to 105 km, and an approximate Gaussian curve was separated from the main sodium layer at 105 to 120 km. We call this separated structure a low thermospheric sodium layer (LTSL). Figure 1b shows the time-altitude variations of the sodium density on 6 July 2010. From 21:05 LT on 6 July 2010 to 00:20 LT on 7 July 2010, the LTSL exists. The main sodium layer was located from approximately 80 to 102 km, and the peak density of the main sodium layer was approximately 2000 cm^{-3}. To start, the LTSL was located at approximately 114 km and the peak density of LTSL was 451 cm^{-3}, which was approximately 25% of the peak density of the main sodium layer. From 21:20 LT to 22:40 LT, the peak altitude of the LTSL descended from 114 to 107 km, with an average downward speed of 5.26 km/h. Afterwards, the LTSL tended to flatten. From 22:40 LT to 00:20 LT, the peak altitude of the LTSL descended from 107 km to 105 km, with an average downward speed of 1.2 km/h. Then, the LTSL gradually faded into the main sodium layer. At 22:15 LT, an SSL appeared at 96 km. The density of the SSL increased from 1200 to 4000 cm^{-3}.

Although LTSLs have been reported at high, middle and low latitude regions, the occurrences of LTSLs are very rare. We selected 38 LTSLs based on 11,607 h of observational data from 2010 to 2016. Table 1 shows the parameters of the LTSLs. We found the time when the LTSL density reached its maximum, this moment is called the peak time and is shown in the second column. The sixth column shows the density of the main sodium layer at the same times. In addition, the last column shows the ratio of the peak density of the LTSL to the peak density of the main sodium layer.

Table 1. List of the low thermospheric sodium layer (LTSL) cases during 2010–2016.

Date	Peak Time (LT)	Peak Altitude (km)	Peak Density (cm^{-3})	FWHM (km)	Peak Density of Main Sodium Layer (cm^{-3})	Ratio
20100427	04:36	110	130	6.8	1648	7.89%
20100512	23:24	115	247	5.4	1659	14.89%
20100522	21:25	111	1004	6.5	1707	58.82%
20100525	22:21	115	236	5.3	1505	15.68%
20100706	21:40	112	451	2.7	1706	26.44%
20101027	19:57	106	286	1.2	4202	6.81%
20110201	22:32	105	536	1.8	4889	10.96%
20110502	22:22	110	86	4.7	1700	5.06%
20110526	20:38	113	410	4.0	1656	24.76%
20110530	22:28	113	201	11.5	1366	14.71%
20110531	22:27	105	272	4.2	2087	13.03%
20110624	23:30	110	882	9.5	1666	52.94%
20110625	21:49	110	652	7.4	1670	39.04%
20110810	22:02	105	183	2.7	2723	6.72%
20110816	22:44	106	140	6.6	2591	5.40%
20120203	23:20	105	253	1.5	3552	7.12%
20120502	23:27	115	219	8.9	2923	7.49%
20120610	23:41	115	137	5.7	1644	8.34%
20120701	21:40	118	198	7	2175	9.10%
20130116	00:12	109	267	3.6	5238	5.10%
20130117	22:51	105	293	4.2	5239	5.59%
20130510	23:42	111	90	5.5	1838	5.00%
20130519	23:10	113	323	3.5	2754	11.73%
20130611	21:38	108	299	4.5	2686	7.41%
20130705	21:21	105	237	1.7	1600	14.81%
20130716	21:17	113	109	5.2	1449	7.52%
20140430	21:06	105	253	1.6	4187	6.04%
20140504	00:23	111	446	6.6	3322	13.43%
20140525	23:51	108	556	3.1	3163	17.58%
20140725	22:36	106	287	1.7	2211	12.98%
20140727	21:57	106	759	2.8	2873	26.00%
20150601	22:44	110	330	9.8	3380	9.76%
20160407	02:12	107	139	0.6	2502	5.56%
20160503	23:01	110	349	2.0	1831	19.06%
20160512	02:16	113	503	10.8	4519	11.13%
20160516	20:07	108	217	1.5	3004	7.22%
20160819	22:41	105	707	4.3	3405	20.76%
20160908	19:50	106	386	3.0	4375	8.82%

Figure 2 shows the statistical results of the parameters of the LTSLs. Figure 2a shows the peak LTSL values located within the altitude range of 105 to 120 km with an average altitude 109.5 km. As shown in Figure 2b, LTSLs occurred from dusk until dawn at any time during the whole night. However, most peak LTSL values occurred at 20:00 LT–00:00 LT. Figure 2c shows the widths of the LTSLs, ranging from 1 to 12 km with an average width of approximately 4.7 km. In addition, most of the LTSL widths were less than 6 km. Figure 2d shows that the peak densities of the LTSLs had extensive variations, ranging from 50 to 1000 cm^{-3}. However, the densities of all the LTSL cases were much less than the densities of main sodium layers.

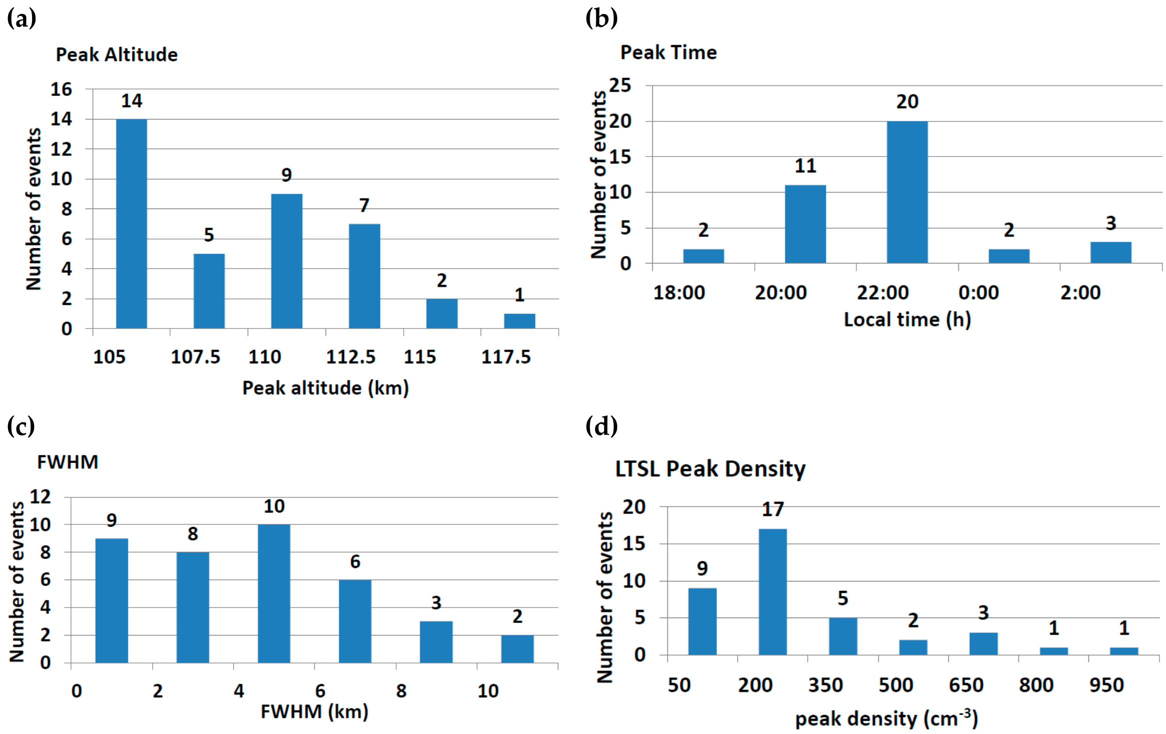

Figure 2. Histogram of (**a**) peak altitudes, (**b**) peak times, (**c**) full width at half maximums (FWHMs), and (**d**) peak densities of LTSLs.

Comparing the statistical parameters of the LTSLs with the statistical parameters of the SSLs observed at Yanqing [11,32], three differences become clear. The altitude of the LTSLs (ranging from 105 to 120 km with an average altitude of 109.5 km) are higher than those of the SSLs (ranging from 90 to 100 km with an average of 95.7 km); the densities of the LTSLs (which are much lower than that of the main sodium layer) are less than those of the SSLs (which are much greater than that of the main sodium layer); and the FWHMs of the LTSLs (distributed from 1 to 12 km with an average width of approximately 4.7 km) are broader than those of the SSLs (approximately 0.2–3.0 km with an average value of 1.7 km). Furthermore, much like the SSLs, most of the LTSLs appeared at approximately 23:00 LT.

3.1.2. The Seasonal Variations of LTSLs

Figure 3a shows the occurrence rates of the LTSLs in each month (the number of LTSL cases/observation hours each month). Figure 3b shows observation time of lidar in each month exceeds 300 h. The seasonal variations of the LTSL occurrences are very obvious. LTSLs are most frequent from May to July and occasionally occurred in April and August. However, in the rest of the months, LTSL occurrences were rare. For instance, in January and February, LTSLs were observed twice in the past seven years. Only one LTSL was observed in September, and only one was observed in October. In March, November and December, we did not observe a single LTSL event. This varying pattern is similar to those reported in the previous works about the SSLs and Es [21,30,35].

(a)

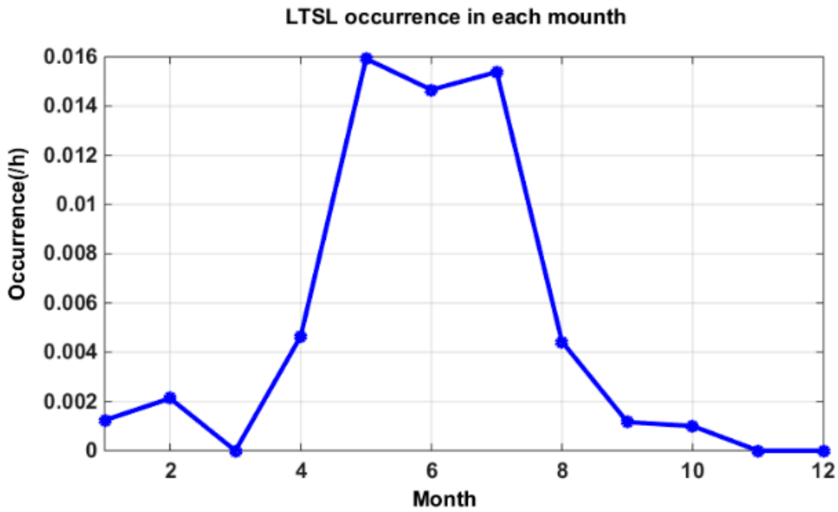

(b)

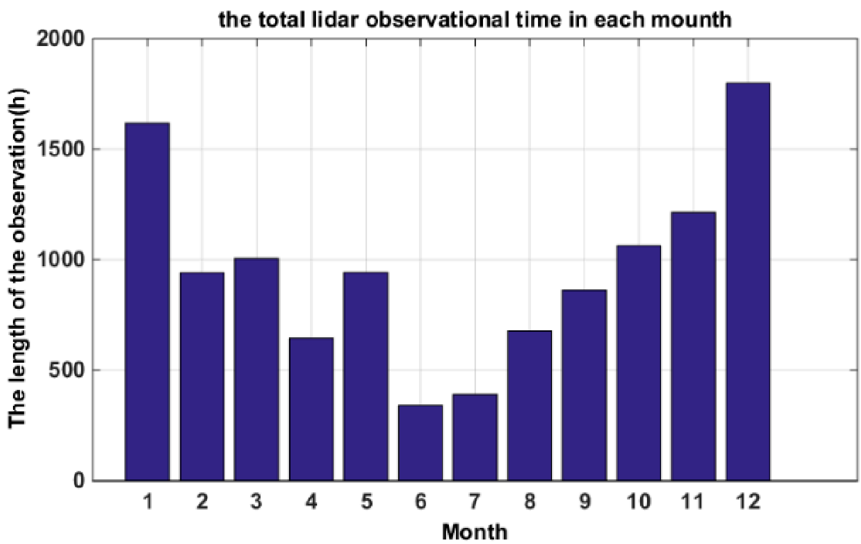

Figure 3. (**a**) The seasonal variations of the LTSL occurrence rates and (**b**) the observation time of lidar in each month.

3.1.3. The Inter-Annual Variation of LTSLs

The occurrences of LTSL in each year are not constant (Figure 4a). Based on seven years of observational data, the occurrences of LTSL and the numbers of sunspot (Figure 4b) are shown to be related. In 2010, 2011, 2013 and 2016, the solar activity was weak, but the LTSL is more frequent. However, in 2012 and 2014, the occurrence rates of LTSLs are lower while the corresponding solar activity is strong. The only exception is 2015: the solar activity of this year was not strong, but only one LTSL case was observed, occurring on 1 June 2015. In July and August of this year, the lidar did not operate as its system was being upgraded. The missing data may be responsible for the lower event occurrence rate in 2015.

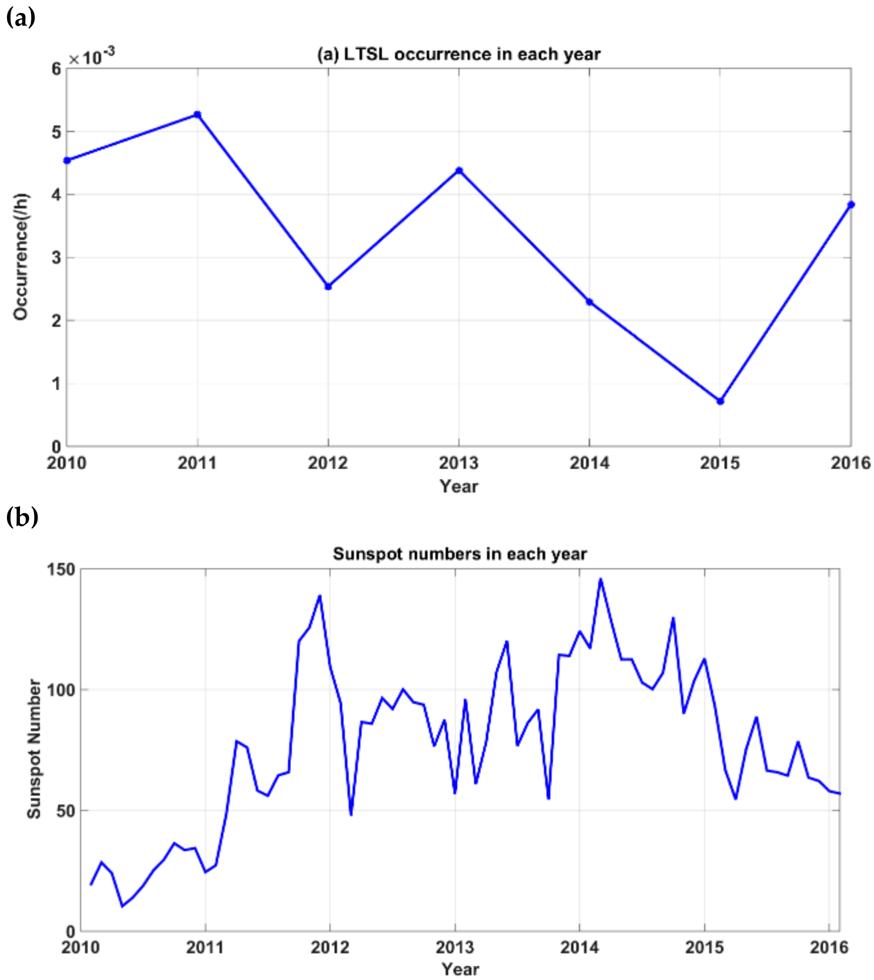

Figure 4. (**a**) The inter-annual variations of LTSL occurrence rates from 2010 to 2016. (**b**) The sunspot numbers from 2010 to 2016.

The occurrences of LTSLs showed a negative correlation with the solar activity. Here, we present a possible explanation from the paper of Dawkins et al. that indicates that the behaviors of the metal layers span longer timescales. On the topside of the sodium layer, sodium ions are formed as a result of both photoionization and charge transfers with ambient ions ((R1)–(R3)) [37]:

$$Na + h\nu \rightarrow Na^{+} + e^{-} \tag{R1}$$

$$Na + NO^{+} \rightarrow Na^{+} + NO \tag{R2}$$

$$Na + O_2^{+} \rightarrow Na^{+} + O_2 \tag{R3}$$

Photoionization and temperature are pronounced with the solar cycle effect [38]. During solar maxima, the rates of photoionization increases, resulting in an enhanced concentration of metal ions due partly to reaction (R1) but more importantly to (R2) and (R3) due to an associated increase in the amount of ambient E region ions and the corresponding increases in the rates of charge transfer reactions. At the same time, the increased concentration of atomic O around solar maximum decreases the rate of neutralization of Na^{+}, because it destroys Na^{+}. N_2 cluster ions which would otherwise dissociative recombine with electrons [15]. Thus, during solar maxima, sodium usually occurs in the form of ions at 110 km. In addition, reduced numbers of LTSL events were observed.

3.2. The Correlation between LTSLs and Es

There are several reports highlighting the simultaneous occurrences of LTSLs and Es layers and pointing to some possible links between the LTSLs and Es layers. The seasonal variations of the LTSLs are extremely similar to those of the Es layers, and the local time variations of the LTSLs lag behind those of the Es layers by approximately 2 h at Utah State University [30]. Case studies reported that the local times, altitudes, and intensities of the LTSLs were highly consistent with the Es layers reported by two examples [20].

In this research, we selected high-altitude Es layers from 2010 to 2016 according to the following criteria. The altitude of the Es layer is higher than 105 km; the Es lasts for at least 1 h; the critical frequency of Es layers is greater than 3.5 MHz.

Figure 5 shows the monthly occurrence rates of LTSLs and Es. Even though the occurrence rate of Es was slightly greater than that of LTSLs, the seasonal variations of the occurrences of LTSLs and Es follow the same trend. Figure 5 indicates the LTSLs and Es mostly occurred between May and August, while a few cases were observed during the winter.

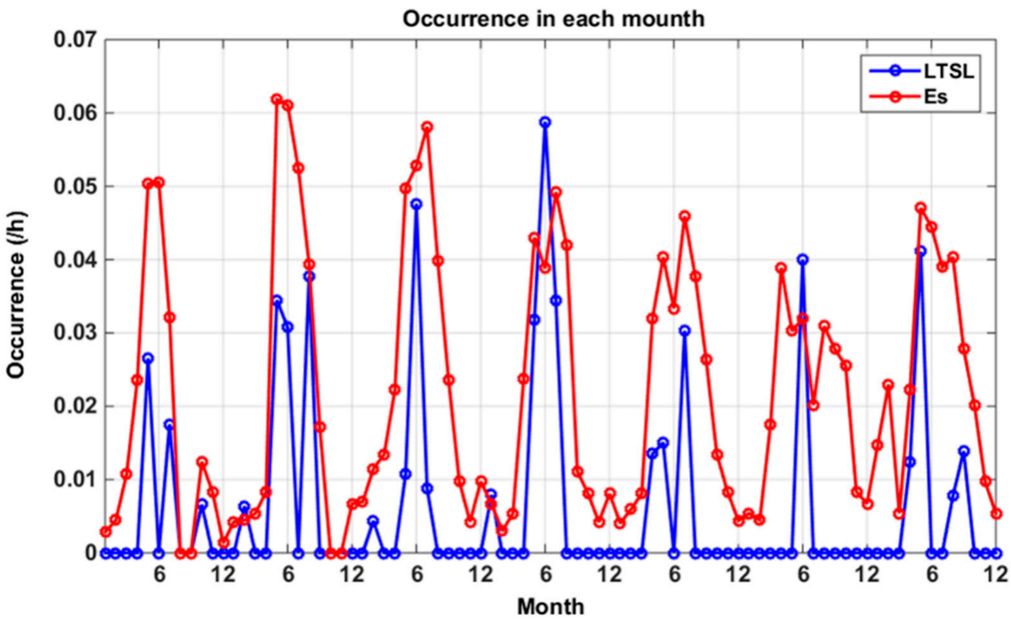

Figure 5. The monthly occurrence rates of LTSLs and Es (occurrence rates = the number of LTSL or Es in each month/the total observational time in each month).

To identify further connections between the LTSLs and Es, we compared the LTSL and Es cases. The data from 2010 to 2015 were used for comparison. A related Es layer was considered that required the observation time of the Es must be within $T_{LTSL} \pm 2$ h, where T_{LTSL} is the start of an LTSL. Of the thirty-eight nights during which the LTSL occurred, there were thirty-six related Es layers. That is, 95% of the LTSL events were accompanied by Es layers. This correlation is greater than that between the SSLs and Es: 87% of the SSLs were accompanied by Es [11]. As shown in Table 2, we listed the height, local times and critical frequencies of thirty-eight Es cases, which mostly occurred close to the beginning of the LTSL events. Table 2 shows that thirty-six Es layers are related to LTSL events (95%). There were only two unrelated events, which occurred on 10 May 2013 and 4 May 2014.

Table 2. The parameters of the Es layers.

Data	Beginning of LTSL (LT)	Es Height (km)	Es Time (LT)	Critical Frequency of Es (MHz)
20100427	3:34	136	02:30	2.51
20100512	22:59	114	21:00	3.7
20100522	21:22	116	20:36	7.9
20100525	20:52	118	21:06	5.85
20100706	21:26	116	21:36	4.2
20101027	19:20	110	19:06	3.8
20110201	18:22	107	19:00	2.99
20110502	21:42	109	20:00	3.3
20110526	20:38	115	21:00	4.55
20110530	21:40	114	21:00	7.15
20110531	22:27	110	21:00	3.05
20110624	21:48	113	21:00	5.55
20110625	21:14	115	21:00	4.75
20110810	21:07	105	22:00	2.75
20110816	21:29	113	20:00	5.4
20120203	23:20	107	23:00	3.48
20120502	21:39	106	21:00	3.48
20120610	23:18	111	23:00	2.91
20120701	21:40	111	20:00	5.1
20130116	23:02	105	21:35	3.67
20130117	22:51	105	21:05	4.25
20130510	22:41	None	None	None
20130519	21:03	113	22:00	5.55
20130611	21:38	113	21:00	8.27
20130705	20:33	120	19:05	3.85
20130716	20:38	112	20:00	12.07
20140430	20:04	113	20:00	2.3
20140504	22:24	None	None	None
20140525	19:24	115	18:00	5.85
20140725	18:30	108	18:00	5.9
20140727	20:36	114	20:00	2.4
20150601	20:53	115	21:00	7.14
20160407	21:16	109	20:00	4.2
20160503	20:03	120	20:00	5.7
20160512	20:13	114	20:00	6.86
20160516	19:47	110	19:00	5.9
20160819	20:08	115	20:00	6.04
20160908	19:36	124	20:00	5.62

Figure 6 shows two typical examples of the close relations between Es and LTSLs. The first occurred on 6 July 2010, and both an LTSL event and Es layer were present during the whole observation period. The other case occurred on 27 October 2010, and both an LTSL event and Es layer appeared before 22:00 LT. At this night, the data were collected from 21:00 LT until the next day at 01:00 LT. The LTSL and Es were both observed throughout the night. The main sodium layer was distributed from 80 to 102 km, with a peak sodium density of 1623 cm^{-3}. At 21:10 LT, the LTSL was extended from 113 to 116 km and was separated from the main sodium layer. The peak density of the LTSL was 118 cm^{-3}, which was approximately 7.3% of the peak density of the main sodium layer. Simultaneously, an Es layer was observed at approximately 115 km with a critical frequency of 4.2 MHz. At 21:30 LT, the peak of the LTSL descend to 112 km, and the peak density reached its maximum. At this time, the peak density of the LTSL was 451 cm^{-3}, which was approximately 44% of the peak density of the main sodium layer. The LTSL descended from 114 to 105 km and merged into the main sodium layer at 00:10 LT. The descent speed was 3.15 km/h. The Es layer also gradually descended to 108 km, and its descent was close to that of the LTSL.

(a)

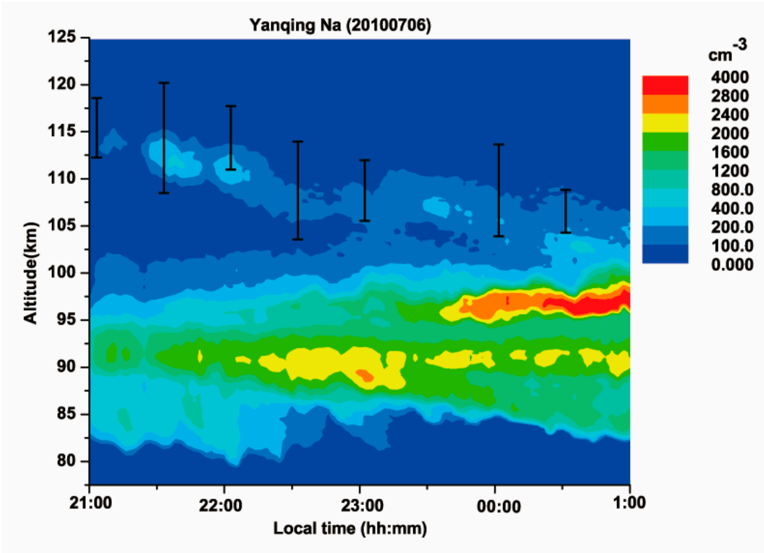

(b)

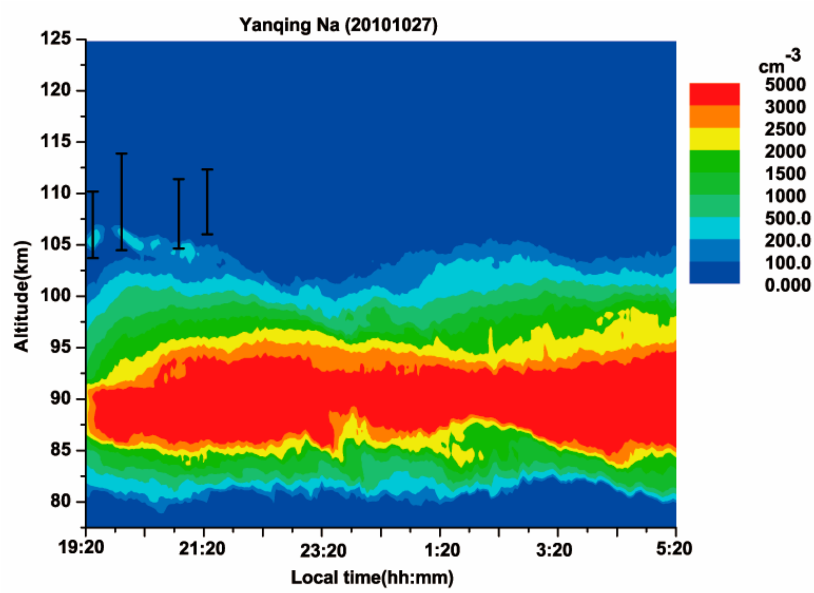

Figure 6. The evolution of the sodium densities and Es on (**a**) 6 July 2010 and (**b**) 27 October 2010. The pseudo color image demonstrates the density evolution of sodium. The central height of the black bar shows the height of the Es, and the length demonstrates the critical frequency of the Es (1 km represents 0.5 MHz).

On the night of 27 October 2010, the data were collected from 19:20 LT until the next day at 05:20 LT. The LTSL and Es were both observed from 19:20 LT to 22:00 LT. The main sodium layer lay between 80 and 103 km with a peak density of 4202 cm^{-3}. At the beginning of the night, the LTSL was located at 105–107.5 km and was separated from the main sodium layer. The LTSL peak density was 286 cm^{-3}, which was approximately 6.8% of the peak density of the main sodium layer. After 19:50 LT, the LTSL started to descend and gradually merge into the main sodium layer. The descent speed was 2.24 km/h. In the first-half of the night, an Es layer occurred at 106 km with the critical frequency of 3.8 MHz.

The Es layer disappeared while the LTSL merged with the main sodium layer. In addition, neither the LTSLs nor the Es was observed after midnight.

Figure 6 shows that in the two cases, the heights and local times of the Es layers are close to the LTSL peaks. We listed the time differences and altitude differences between the LTSL and Es. Figure 7 shows that for most cases, the local times, altitudes, and densities of the LTSLs were relevant to those of the Es. Most of the LTSLs and Es were observed within the range of 105–125 km, with average altitudes of 109.5 km and 112.5 km, respectively. The difference of the average altitudes of SSL and Es was approximately 10 km [11], while that between LTSL and Es was only 3 km. In thirty-four cases, the height differences between the LTSL peaks and Es were less than 10 km (94%). Among these, there were twenty-five cases in which the height differences between the LTSL peaks and Es were less than 5 km (70%). In addition, there are twenty-nine cases wherein the Es were higher than the LTSLs (81%; shown in Figure 7a). The differences of the occurrence times between the LTSLs and Es were less than 120 min, and most of the Es layers occurred a little earlier. There are fifteen Es and LTSL cases with formations within half an hour (42%), and the time intervals of the fourteen Es and LTSL cases were a half-hour to an hour (39%). In addition, the time intervals of five Es and LTSL cases were approximately an hour to hour and a half (14%). Only two Es layers occurred more than ninety minutes before the LTSLs (shown in Figure 7b). In Figure 7c, the horizontal axis represents the peak density of the LTSLs, and the vertical axis represents the critical frequency of the Es. An increased density of the LTSL corresponds to an increased critical frequency of the Es, especially when the density was less than 600 cm^{-3}. The high correlation between LTSLs and Es implies that LTSLs are likely directly transformed from the sodium ions in Es or Es and LTSLs are probably from the same source.

However, there are two LTSL cases observed without Es layer. Figure 8 shows an example on 10 May 2013, the LTSL appeared before 23:00 LT, and there were no Es layers before and after three hours shown in Figure 8c,d. This observation indicated LTSL had weak correlation to Es in some cases. The temperature-controlled theory was first proposed by Zhou et al., which suggested the triggering of sodium atoms by some means through temperature enhancement in a narrow altitude region due to energy damping during gravity wave breaking [39]. Recently, an empirical model was proposed that sodium species were collected by an icy-dust reservoir and stored during the extremely cold phase (<150 K) and a large temperature enhancement (>40 K of temperature increase) triggered a generation of sodium atoms [40]. Therefore, we turn to the temperature profiles from SABER. We found that three hours before this LTSL, an extremely low temperature was observed by SABER. The minimum temperature dipped as low as 140 K at 103 km at 17:36 LT (LT = UT + 8) on 10 May 2013 was shown in Figure 8b. After about two hours, the temperature raised above 222 K in this range. At 105 km, the temperature raised from 159 K to 264 K, the temperature enhancement was 105 K which is much higher than 40 K. This event provides evidence that the possibility of an icy-dust layer acting as the sodium reservoir and then releasing the gathered sodium during a large temperature enhancement. Moreover, the other LTSL on 4 May 2014, a large temperature enhancement was also present, the temperature raised from 206 K to 277 K at 105 km from 19:30 LT to 21:25 LT. However, the lowest temperature was 169 K at 102 km, is higher than previous reported extremely cold phase 150 K [40] for ice dust. Although tidal waves or other such reasons can have amplitude of 40–60 K in the MLT region. The LTSLs during large temperature enhancement suggesting that we cannot ignore other mechanisms such as the release of free sodium atoms from the dusty surfaces.

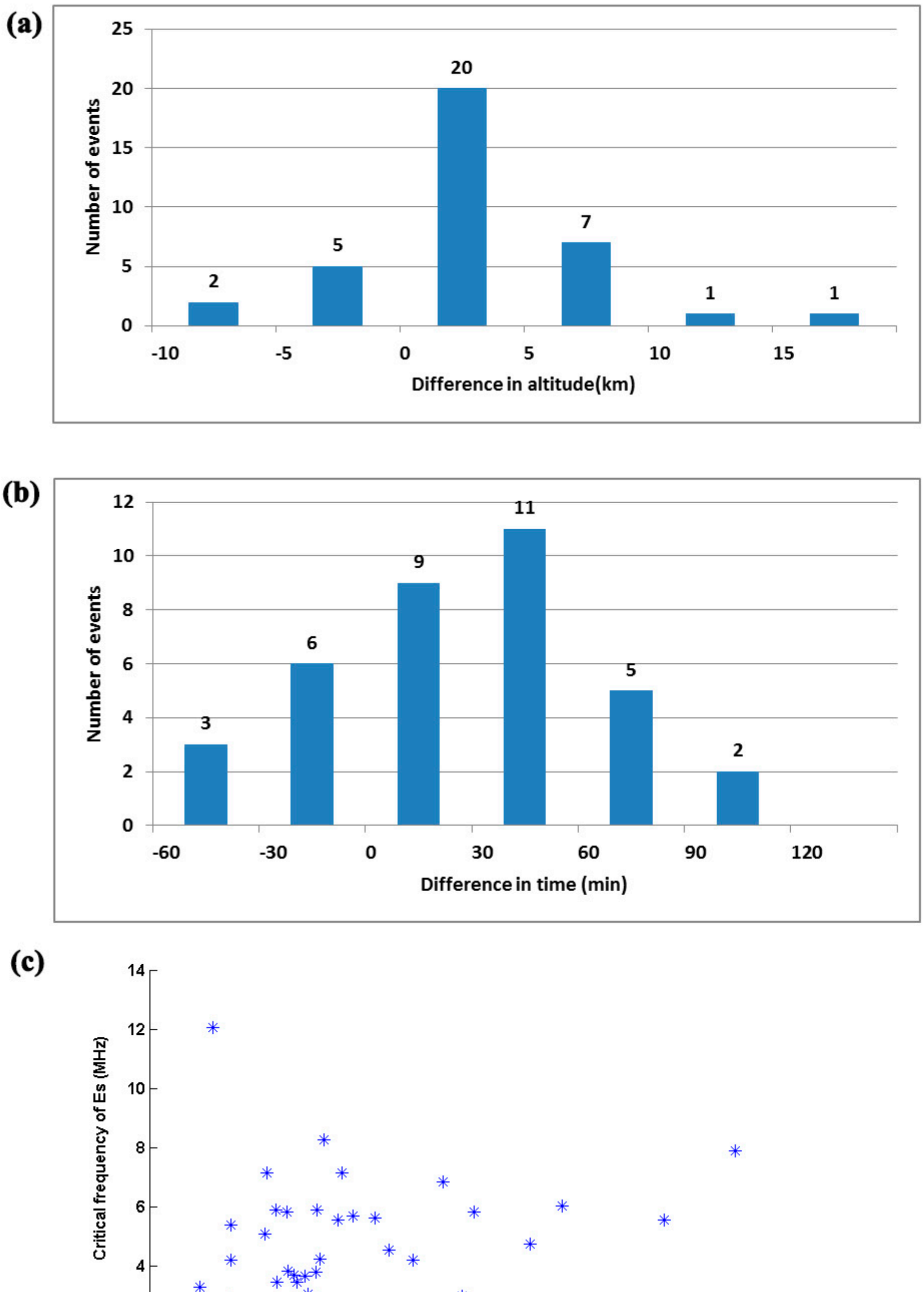

Figure 7. (**a**) The altitude of Es versus LTSL (positive number indicates that Es higher than LTSL), (**b**) the local time of the Es versus LTSL (positive number indicates that Es occurred earlier than LTSL) and (**c**) the intensity of the Es versus LTSL.

(a)

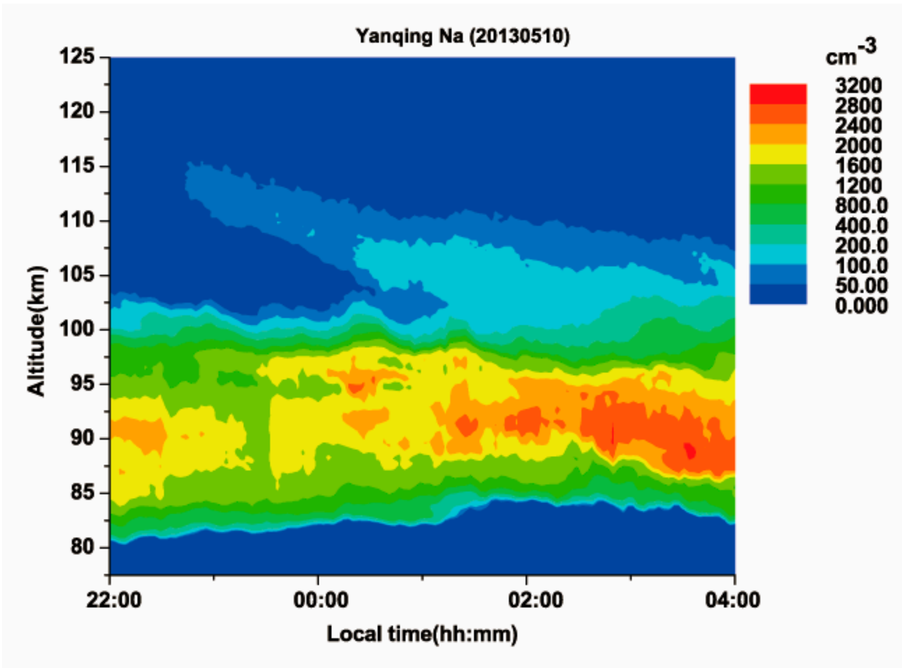

(b)

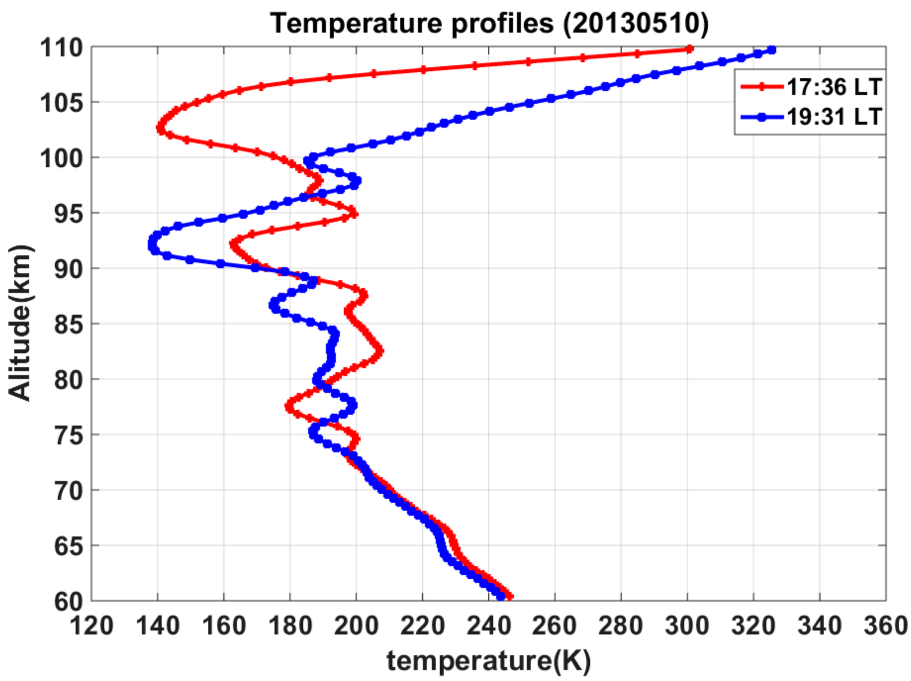

Figure 8. *Cont.*

(c)

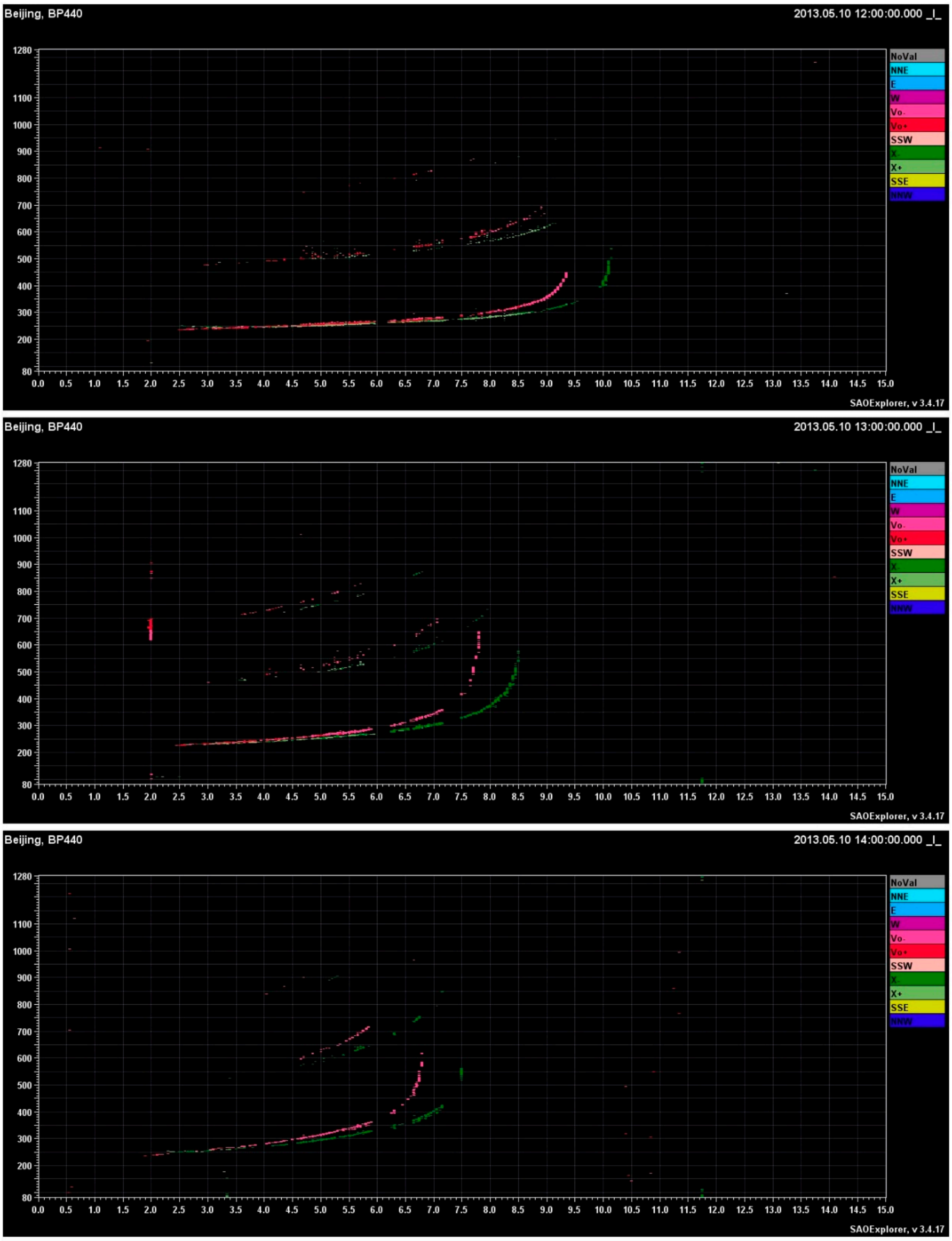

Figure 8. *Cont.*

(d)

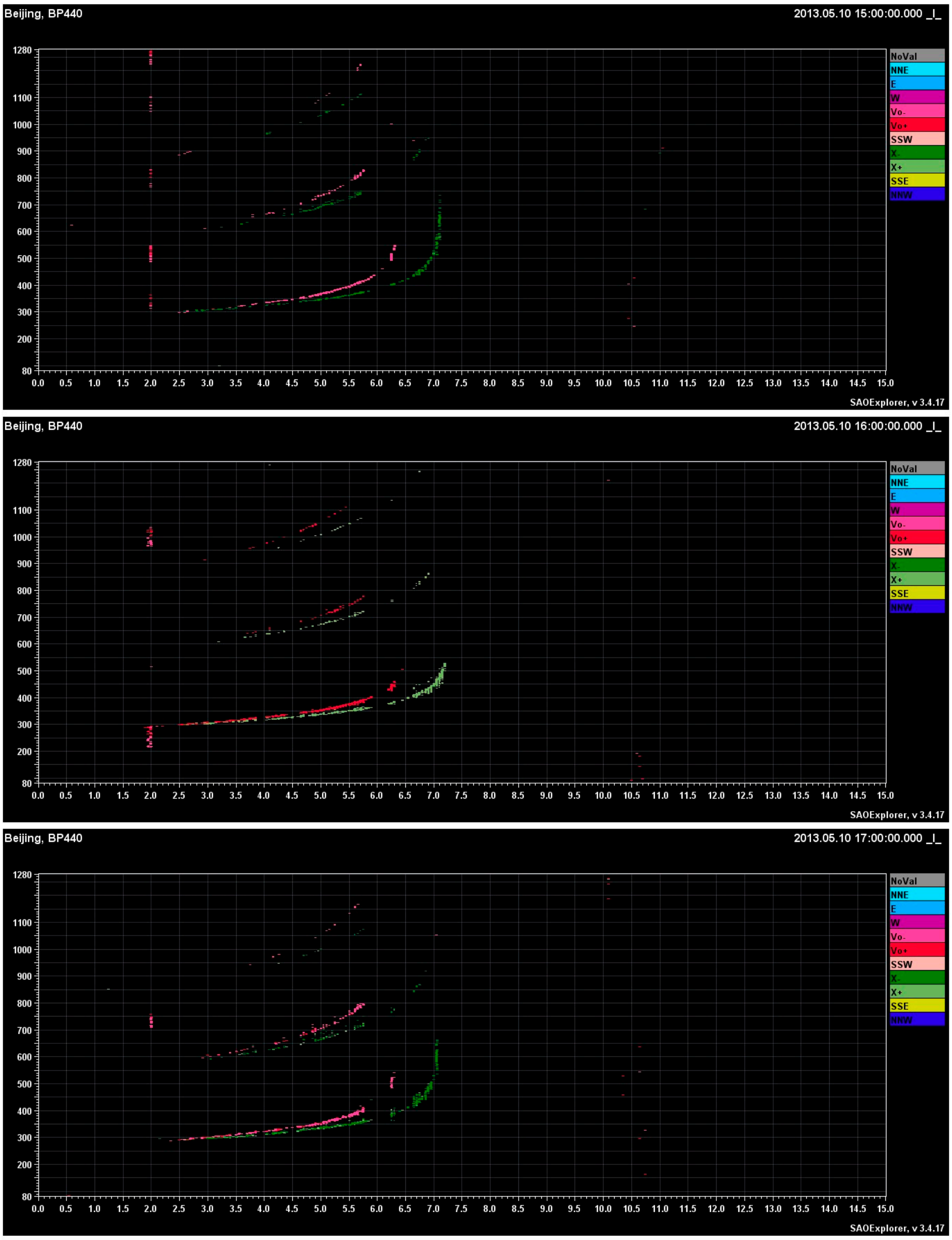

Figure 8. (**a**,**c**,**d**) The evolution of sodium densities and ionogram on 10 May 2013. (**b**) Temperature profiles before the LTSLs, with an extremely low temperature of 140 K at 103 km at 17:36 LT (LT = UT + 8) on 10 May 2013.

3.3. The Correlation between LTSLs and Tidal Wave

The early observations indicated some possible relationships among the LTSL, Es and tides. The zonal tidal wind in the Es region could produce thin metal ions layers through wind shearing, and these metal ions descended over time as the phases of the winds changed [41]. Xue et al. reported two sodium layers located near 120 km that displayed a tide-induced downward motion [20]. These results indicated that the relationship among tidal wave, Es layer and LTSL. The descending rates of the thermospheric metal layers are consistent with the phase speeds of the semidiurnal tides [24,28]. To explore the link between LTSLs and tidal wave, we analyzed the LTSLs and tides from 2010 to 2015 (with an absence of observational data occurring on 6 July 2010).

A harmonic analysis was applied to the three days of data to deduce the prevailing zonal wind velocity, as well as the amplitudes and phases of the harmonic components. Y = $y0 + \alpha 1\cos(2\pi t/24 + \varphi 1)$ + a2cos($2\pi t/12 + \varphi 2$)+ $\alpha 3\cos(2\pi t/8 + \varphi 3)$ + a4cos($2\pi t/6 + \varphi 4$), where y is the wind velocity; $y0$ is the background wind; and $\alpha 1$,$\alpha 2$,$\alpha 3$, and $\alpha 4$ are the amplitudes in m/s. $\varphi 1$, $\varphi 2$, $\varphi 3$, and $\varphi 4$ are the phases and are given by the local solar time in hours of the maximum flow in the eastward direction of the tidal velocities [42].

We analyzed 31 cases of zonal wind from the meteor radar observations. The third column of Table 3 represents the dominant tidal components (downward trend phase and maximum amplitude): 24 h (diurnal tide), 12 h (semidiurnal tide), 8 h (terdiurnal tide) and 6 h (quardiurnal tide). The fourth column represents the dominant tidal descent speed. The "-" shows those days with no phase component of the downward trend. The second column represents the descent speed of the LTSL, and "-" indicates no downward movement. There were 22 LTSLs that were observed to descend. We found that every LTSL with a downward trend was accompanied by a descending tidal component, except for that of 1 July 2012. In addition, 38% of the descending LTSL cases were affected by diurnal tides, 33% of the descending LTSL cases were influenced by the semidiurnal tides and 24% of the descending LTSL cases were subjected to terdiurnal tides. These high correlations of the LTSLs and tidal components confirmed that the tidal components of the zonal wind affect the evolution of LTSLs. In Figure 9, the horizontal axis represents the speed of the LTSL descent, and the vertical axis represents the phase speed of the dominant tidal component. The blue circles represent the relationship between the diurnal tide and LTSL. The red stars represent the relationship between the semidiurnal tide and LTSL. In addition, the black diamonds represent the relationship between terdiurnal tide and LTSL. Thus, most LTSL speeds are shown to be similar to those of the tidal components.

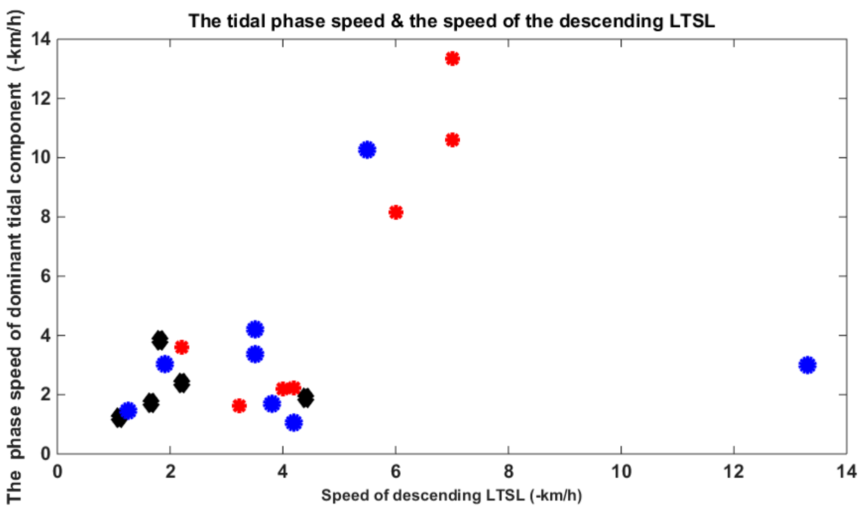

Figure 9. The tidal phase speed versus the speed of the descending LTSL ("−km/h": negative means downward).

Furthermore, there were 10 LTSLs that from their formation to disappearance presented no descending or upward trends and were located in the same altitude zones. Base on Tables 1 and 3, all of these ten LTSLs have two characteristics: the one is that they distribute at low altitude, the other is that they have low density. The formation of these LTSLs may not affected by tidal wave, but overturning from main sodium layer directly. Figure 10 shows that on 25 July 2014 at 21:05 LT, the LTSL appeared at approximately 106 km, and at 24:00 LT, the LTSL suddenly disappeared at approximately 106 km.

In this appearance, we cannot see any downward or upward trends. However, at approximately 2:10 LT, the LTSL appeared again, and lasted until the end of the observational period. Additionally, no downward or upward trends can be seen during its second appearance.

Table 3. The parameters of zonal wind.

Date	Speed of Descending LTSL (−km/h)	Dominant Tidal Component	Phase Speed of Dominant Tidal Component (−km/h)
20100427	-	24 h	1
20100512	3.36	24 h	3.5
20100522	1.96	8 h	4.4
20100525	10.59	12 h	7
20100706	3.15	No data	No data
20101027	2.24	12 h	4.2
20110201	-	12 h	5.25
20110502	-	24 h	2.34
20110526	1.47	24 h	1.25
20110530	1.71	8 h	1.67
20110531	-	-	-
20110624	-	12 h	10
20110625	10.27	24 h	5.5
20110810	-	24 h	5
20110816	3	24 h	13.3
20120203	1.07	24 h	4.2
20120502	2.19	12 h	4
20120610	1.23	8 h	1.1
20120701	2.31	-	-
20130116	8.14	12 h	6
20130117	1.62	12 h	3.23
20130510	3.6	12 h	2.2
20130519	4.22	24 h	3.5
20130611	1.7	24 h	3.8
20130705	-	24 h	3
20130716	-	12 h	5
20140430	13.34	12 h	7
20140504	3.84	8 h	1.82
20140525	3.02	24 h	1.9
20140725	-	6 h	4
20140727	2.4	8 h	2.2
20150601	-	24 h	4.67

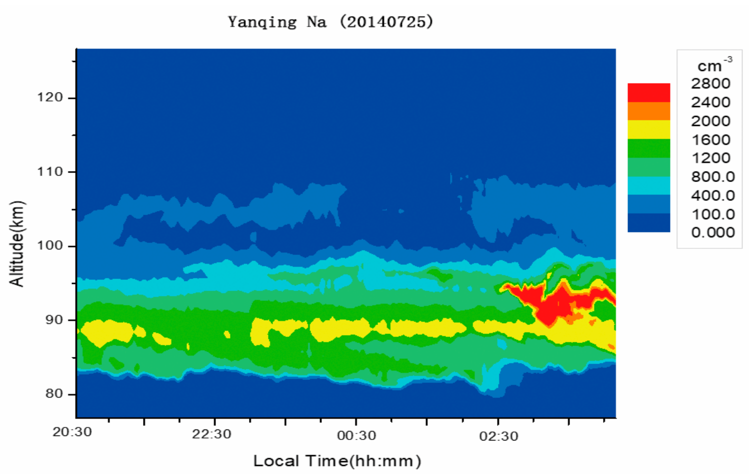

Figure 10. Time-altitude variations of the sodium densities on 25 July 2014.

4. Summary

In recent years, metal atoms above 105 km have attracted widespread interest. Some case studies indicated that Es plays a crucial role in producing metal atoms. Based on the 11,607 h of observational data from 2010 to 2016 from Yanqing, China, we found 38 LTSL cases. The statistical studies of the peak altitudes, peak times, and peak densities of the LTSL indicate that the LTSL occurred infrequently at relatively high altitudes with smaller densities and, broader FWHMs. The occurrences of these phenomena exhibited a maximum near 23:00 LT. The seasonal variations and inter-annual variations are dramatic. The occurrences of LTSLs were mainly concentrated in May, June and July. In addition, the occurrences of LTSLs and the numbers of sunspots had clear negative correlations. From the statistical results concerning the LTSLs and Es over the six studied years, the trends of the occurrences of LTSLs and Es are shown to be very similar. Using a case by case comparison, we found that more than 90% the LTSLs were related to Es. Furthermore, approximately 70% of the LTSLs displayed downward trends, and tidal components played a key role in these downward processes. The Es are known to be thin layers composed of various metallic ions. Recently, a new lidar has been constructed by the Meridian Space Weather Monitoring Project to simultaneously detect calcium atoms and calcium ions. If we simultaneously observed enhanced calcium atoms and reduced calcium ions, the correlation between metal ions and metal atoms would be clearer.

Author Contributions: Conceptualization, G.Y.; methodology, Y.X.; software, Y.X.; validation, G.Y.; formal analysis, G.Y.; investigation, Y.X.; resources, G.Y. and J.W.; data curation, J.W., L.D., X.C., F.L.; writing—original draft preparation, Y.X. and G.Y.; writing—review and editing, Z.W., J.J. and X.Z.; visualization, Y.X.; project administration, G.Y.; funding acquisition, G.Y. All authors have read and agreed to the published version of the manuscript.

Funding: This research was funded by the Natural Science Foundation of China, grant number 41474130, 41627804 and 41604130; Beijing Science and Technology Plan, grant number Z181100002918001. This research was also supported by National Space Science Center research fund for key development directions, and the Specialized Research Fund for State Key Laboratories of China.

Acknowledgments: We sincerely acknowledge Meridian Space Weather Monitoring Project (http://data.meridianproject.ac.cn/), Institute of Geology and Geophysics, Chinese Academy of Science ((http://geospace.geodata.cn/),) and World Data Center for the Production, Preservation and Dissemination of the International Sunspot Number (http://www.sidc.be/silso/home) providing data.

Conflicts of Interest: The authors declare no conflict of interest.

References

1. Slipher, V.M. Emission in the spectrum of light in the night sky. *Publ. Astron. Soc. Pac.* **1929**, *242*, 262–263.
2. Plane, J.M.; Feng, W.; Dawkins, E.C. The mesosphere and metals: Chemistry and changes. *Chem. Rev.* **2015**, *115*, 4497–4541. [CrossRef] [PubMed]
3. Clemesha, B.R.; Kirchhoff, V.; Simonich, D.; Takahashi, H. Evidence of an extra-terrestrial source for the mesospheric sodium layer. *Geophys. Res. Lett.* **1978**, *5*, 873–876. [CrossRef]
4. Heinselman, C.J.; Thayer, J.P.; Watkins, B.J. A high-latitude observation of sporadic sodium and sporadic E-layer formation. *Geophys. Res. Lett.* **1998**, *25*, 3059–3062. [CrossRef]
5. Fan, Z.Y.; Plane, J.M.C.; Gumbel, J. On the global distribution of sporadic sodium layers. *Geophys. Res. Lett.* **2007**, *34*. [CrossRef]
6. Williams, B.P.; Berkey, F.T.; Sherman, J.; She, C.Y. Coincident extremely large sporadic sodium and sporadic E layers observed in the lower thermosphere over Colorado and Utah. *Ann. Geophys.* **2007**, *25*, 3–8. [CrossRef]
7. Simonich, D.; Clemesha, B. Sporadic sodium layers and the average vertical distribution of atmospheric sodium: Comparison of different Nas layer strengths. *Adv. Space Res.* **2008**, *42*, 229–233. [CrossRef]
8. Dou, X.; Xue, X.; Li, T.; Chen, T.; Chen, C.; Qiu, S. Possible relations between meteors, enhanced electron density layers, and sporadic sodium layers. *J. Geophys. Res. Space Phys.* **2010**, *115*. [CrossRef]
9. Tsuda, T.T.; Nozawa, S.; Kawahara, T.D.; Kawabata, T.; Saito, N.; Wada, S.; Hall, C.M.; Oyama, S.; Ogawa, Y.; Suzuki, S.; et al. Fine structure of sporadic sodium layer observed with a sodium lidar at Tromsø, Norway. *Geophys. Res. Lett.* **2011**, *38*. [CrossRef]

10. Takahashi, T.; Nozawa, S.; Tsuda, T.T.; Ogawa, Y.; Saito, N.; Hidemori, T.; Kawahara, T.D.; Hall, C.; Fujiwara, H.; Matuura, N.; et al. A case study on generation mechanisms of a sporadic sodium layer above Tromsø (69.6° N) during a night of high auroral activity. *Ann. Geophys.* **2015**, *33*, 941–953. [CrossRef]
11. Jiao, J.; Yang, G.; Zou, X.; Gong, S.; Wang, J.; Tian, D.; Zhang, W.; Zhang, T.; Yang, X.; Fu, J.; et al. Joint observations of sporadic sodium and sporadic E layers at middle and low latitudes in China. *Chin. Sci. Bull.* **2014**, *59*, 3868–3876. [CrossRef]
12. Nagasawa, C.; Abo, M. Lidar observation of a lot of sporadic sodium layers in mid-latitude. *Geophys. Res. Lett.* **1995**, *22*, 263–266. [CrossRef]
13. Clemesha, B.R.; Batista, P.P.; Simonich, D.M. Formation of sporadic sodium layers. *J. Geophys. Res. Space Phys.* **1996**, *101*, 19701–19706. [CrossRef]
14. Kirkwood, S.; von Zahn, U. On the role of auroral electric fields in the formation of low altitude sporadic-E and sudden sodium layers. *J. Atmos. Terr. Phys.* **1991**, *53*, 389–407. [CrossRef]
15. Cox, R.M.; Plane, J.M.C. An ion-molecule mechanism for the formation of neutral sporadic Na layers. *J. Geophys. Res.* **1998**, *103*, 6349–6359. [CrossRef]
16. Collins, S.C.; Plane, J.M.C.; Kelley, M.C.; Wright, T.G.; Soldán, P.; Kane, T.J. A study of the role of ion–molecule chemistry in the formation of sporadic sodium layers. *J. Atmos. Sol. Terr. Phys.* **2002**, *64*, 845–860. [CrossRef]
17. Collins, S.C.; Hallinan, T.J.; Smith, R.W. Lidar observations of a large high-altitude sporadic Na during active aurora. *Geophys. Res. Lett.* **1996**, *23*, 3655–3658. [CrossRef]
18. Gong, S.; Yang, G.; Wang, J.; Cheng, X.; Li, F.; Wan, W. A double sodium layer event observed over Wuhan, China by lidar. *Geophys. Res. Lett.* **2003**, *30*. [CrossRef]
19. Wang, J.; Yang, Y.; Cheng, X.; Yang, G.; Song, S.; Gong, S. Double sodium layers observation over Beijing, China. *Geophys. Res. Lett.* **2012**, *39*, L15801. [CrossRef]
20. Xue, X.; Dou, X.-K.; Lei, J.; Chen, J.S.; Ding, Z.H.; Li, T.; Gao, Q.; Tang, W.W.; Cheng, X.W.; Wei, K. Lower thermospheric-enhanced sodium layers observed at low latitude and possible formation: Case studies. *J. Geophys. Res. Space Phys.* **2013**, *118*, 2409–2418. [CrossRef]
21. Dou, X.; Qiu, S.; Xue, X.; Chen, T.; Ning, B. Sporadic and thermospheric enhanced sodium layers observed by a lidar chain over China. *J. Geophys. Res. Space Phys.* **2013**, *118*, 6627–6643. [CrossRef]
22. Ma, Z.; Wang, X.; Chen, L.; Wu, J. First report of sporadic Na layers at Qingdao (36° N, 120° E), China. *Ann. Geophys.* **2014**, *32*, 739–748. [CrossRef]
23. Tsuda, T.T.; Chu, X.; Nakamura, T.; Ejiri, M.K.; Kawahara, T.D.; Yukimatu, A.S.; Hosokawa, K. A thermospheric Na layer event observed up to 140 km over Syowa Station (69.0° S, 39.6° E) in Antarctica. *Geophys. Res. Lett.* **2015**, *42*, 3647–3653. [CrossRef]
24. Gao, Q.; Chu, X.; Xue, X.; Dou, X.; Chen, T.; Chen, J. Lidar observations of thermospheric Na layers up to 170 km with a descending tidal phase at Lijiang (26.7° N, 100.0° E), China. *J. Geophys. Res. Space Phys.* **2015**, *120*, 9213–9220. [CrossRef]
25. Alan, Z.; Guo, Y.; Vargas, F.; Swenson, G. Firstmeasurement of horizontal wind and temperature in the lower thermosphere (105–140 km) with a Na Lidar at Andes Lidar Observatory. *Geophys. Res. Lett.* **2016**, *43*, 2374–2380. [CrossRef]
26. Xun, Y.; Yang, G.; She, C.-Y.; Wang, J.; Du, L.; Yan, Z.; Yang, Y.; Cheng, X.; Li, F. The first concurrent observations of thermospheric Na layers from two nearby central midlatitude lidar stations. *Geophys. Res. Lett.* **2019**, *46*, 1892–1899. [CrossRef]
27. Chu, X.; Yu, Z.; Gardner, C.S.; Chen, C.; Fong, W. Lidar observations of neutral Fe layers and fast gravity waves in the thermosphere (110–155 km) at McMurdo (77.8° S, 166.7° E), Antarctica. *Geophys. Res. Lett.* **2011**, *38*. [CrossRef]
28. Friedman, J.S.; Chu, X.; Brum, C.G.M.; Lu, X. Observation of a thermospheric descending layer of neutral K over Arecibo. *J. Atmos. Sol. Terr. Phys.* **2013**, *104*, 253–259. [CrossRef]
29. Raizada, S.; Brum, C.M.; Tepley, C.A.; Lautenbach, J.; Friedman, J.S.; Mathews, J.; Djuth, F.T.; Kerr, C. First simultaneous measurements of Na and K thermospheric layers along with TILs from Arecibo. *J. Geophys. Res. Space Phys.* **2015**, *42*, 106–112. [CrossRef]
30. Yuan, T.; Wang, J.; Cai, X.; Sojka, J.; Rice, D.; Oberheide, J.; Criddle, N. Investigation of the seasonal and local time variations of the high-altitude sporadic Na layer (Nas) formation and the associated midlatitude descendingElayer (Es) in lowerEregion. *J. Geophys. Res. Space Phys.* **2014**, *119*, 5985–5999. [CrossRef]

31. Cai, X.; Yuan, T.; Eccles, J.V. A numerical investigation on tidal and gravity wave contributions to the summer time Na variations in the midlatitude E region. *J. Geophys. Res. Space Phys.* **2017**, *122*, 10577–10595. [CrossRef]
32. Cai, X.; Yuan, T.; Pedatella, N.M.; Ban, C.; Liu, A.Z. A Numerical Investigation on the Variation of Sodium ion and observed Thermospheric Sodium Layer at Cerro Pachón, Chile during Equinox. *J. Geophys. Res. Space Phys.* **2019**, *124*, 10395–10414. [CrossRef]
33. Chu, X.; Yu, Z. Formation mechanisms of neutral Fe layers in the thermosphere at Antarctica studied with a thermosphere-ionosphere Fe/Fe^+ (TIFe) model. *J. Geophys. Res. Space Phys.* **2017**, *122*, 6812–6848. [CrossRef]
34. Wang, C. Development of the Chinese Meridian Project. *Chin. J. Space Sci.* **2010**, *30*, 382–384.
35. Jiao, J.; Yang, G.; Wang, J.; Cheng, X.; Li, F.; Yang, Y.; Gong, W.; Wang, Z.; Du, L.; Yan, C.; et al. First report of sporadic K layers and comparison with sporadic Na layers at Beijing, China (40.6° N, 116.2° E). *J. Geophys. Res. Space Phys.* **2015**, *120*, 5214–5225. [CrossRef]
36. Wang, Z.; Yang, G.; Wang, J.; Yue, C.; Yang, Y.; Jiao, J.; Du, L.; Cheng, X.; Wang, C. Seasonal variations of meteoric potassium layer over Beijing (40.41°N, 116.01°E). *J. Geophys. Res. Space Phys.* **2017**, *122*, 2106–2118. [CrossRef]
37. Dawkins, E.C.M.; Plane, J.M.C.; Chipperfield, M.P.; Feng, W.; Marsh, D.R.; Höffner, J.; Janches, D. Solar cycle response and long-term trends in the mesospheric metal layers. *J. Geophys. Res. Space Phys.* **2016**, *121*, 7153–7165. [CrossRef]
38. Forbes, J.M.; Zhang, X.; Marsh, D.R. Solar cycle dependence of middle atmosphere temperatures. *J. Geophys. Res. Atmos.* **2014**, *119*, 9615–9625. [CrossRef]
39. Zhou, Q.; Mathews, J.; Tepley, C. A proposed temperature dependent mechanism for the formation of sporadic sodium layers. *J. Atmos. Terr. Phys.* **1993**, *55*, 513–521. [CrossRef]
40. Qiu, S.; Soon, W.; Xue, X.; Li, T.; Wang, W.; Jia, M.; Ban, C.; Fang, X.; Tang, Y.; Dou, X. Sudden sodium layers: Their appearance and disappearance. *J. Geophys. Res. Space Phys.* **2018**, *123*, 5102–5118. [CrossRef]
41. Chimonas, G. Enhancement of sporadic E by horizontal transport within the layer. *J. Geophys. Res.* **1971**, *76*, 4578–4586. [CrossRef]
42. Batista, P.P.; Clemesha, B.R.; Tokumoto, A.S.; Lima, L.M. Structure of the mean winds and tides in the meteor region over Cachoeira Paulista, Brazil (22.7° S, 45° W) and its comparison with models. *J. Atmos. Sol. Terr. Phys.* **2004**, *66*, 623–636. [CrossRef]